American Journal of Condensed Matter Physics 2013, 3(5): 151-162
DOI: 10.5923/j.ajcmp.20130305.06

First Principles Study of Structural, Electronic and Optical Properties of the Fluoroperovskite $RbCaF_3$ Crystal

Ahmad. A. Mousa[1,*], Jamil M. Khalifeh[2], Nada T. Mahmoud[2], Hassan K. Juwhari[2]

[1]Middle East University, 11831- Amman, P.O. Box 383, Jordan
[2]Physics Department, The University of Jordan, 11942-Amman, Jordan

Abstract The structural, electronic, and optical properties of crystalline fluoroperovskites $RbCaF_3$ were investigated using full potential linearized augmented plane wave (FP-LAPW) method with the generalized gradient approximation (WC-GGA), generalized gradient approximation (PBE-GGA), and the local density approximation (LDA). A detailed comparison between pre-existing calculated values, experimental measurements, and results obtained from previous theoretical studies is provided. The contribution of the electronic states to simplify the optical properties is discussed. In these calculations, it is shown that this structure has indirect energy band-gap (M-Γ). A theoretical study of the high hydrostatic pressure dependence of the electronic properties of the fluoroperovskites $RbCaF_3$ is also presented here. The dielectric function, the refractive index, the absorption coefficient, and the reflectivity are calculated and presented as well.

Keywords The Fluoroperovskite, DFT, GGA, Optical Properties, Band Gap

1. Introduction

The prototype compound of the perovskite structure is $^{XII}Ca^{2+}\ ^{VI}Ti^{4+}\ O^{2-}_3$. The structure is cubic, space group $Pm\bar{3}m$ with one formula unit per unit cell. It is very clear that the two cations are of different covalencies and sizes with the oxygen ions bonding to both. The perovskite structure like many other structures is extremely tolerant of many types of ionic substitution with only requirement that the local charge balance be maintained[1,2]. In the present work, the fluoroperovskite is derived by replacing the O^{2-} ions by the F^- ions. The unbalanced negative charge is compensated by completely replacing all of the smaller 12 coordinated Ca and larger 6 coordinated Ti cations by the mono- and divalent Rb and Ca cations, respectively[3].

Compounds with this structure have received recently increased attention from the scientific community because of their relatively simple crystal structure accompanied by astonishing desired physical properties. Perovskite materials exhibit many interesting and intriguing properties from both the theoretical and application point of view including Colossal magnetoresistance, ferroelectricity,superconductivity, charge ordering, spin dependent transport, high thermo-power and the interplay of structural, magnetic and transport properties that are commonly observed in this family. These compounds are frequently utilized as sensors and catalyst electrodes in certain types of fuel cells, candidates for memory devices and spintronics applications, and a multitude of dielectric properties which are of great importance in the microelectronics and telecommunication industries[4-6].

The compound can be synthesized, as proposed by Bouamrane *et al*[7], by mixing alkali metal and alkaline earth metals with fluorine through the following reaction:

$$3AF + B \rightarrow ABF_3 + 2A$$

Another method, proposed by Ludekens *et al*[8], includes mixing metal halide with alkaline metal oxides as summarized by the following equation:

$$3AF + BO \rightarrow ABF_3 + A_2O$$

Where A and B are the alkali metals and alkaline earth metals, respectively.

The wide-band-gap fluorides are one of the most promising candidates. They offer the possibility of being alloyed to form complex materials with lattice-matched crystal structures and wide band gaps, hence allowing for band-gap engineering and lattice matching[3]. As the growth of high-quality bulk fluoride crystals has been successfully demonstrated in $LiCaAlF_6$, $KMgF_3$, and $LiBaF_3$[9-11], it is only reasonable to extend an investigation to explore the possibilities of actual band structure design with the appropriate lattice-matched substrate selection using ab initio calculations within the local density approximation (LDA)[3].

This paper is organized in four sections. Section 2 is

* Corresponding author:
amousa@meu.edu.jo (Ahmad. A. Mousa)
Published online at http://journal.sapub.org/ajcmp

devoted to the method of calculation, section 3 deals with the results and discussion, and in section 4 we present the conclusion.

2. Computational Method

We performed a total energy calculation for the fluoroperovskite, $RbCaF_3$, cubic structure which contains only one molecule composed of four atoms in its unit cell. The Rb, Ca and F atoms are positioned at 1a (0, 0, 0), 1b (½, ½, ½) and 3c (0, ½, ½) sites of Wyckoff coordinates, respectively. Figures 1 (a and b) show a unit cell and the first Brillouin zone of $RbCaF_3$, respectively.

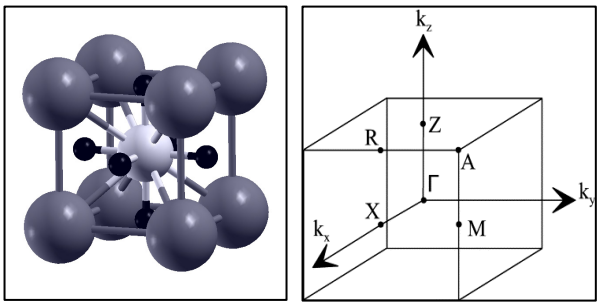

a) b)

Figure 1. a) Crystal structures of $RbCaF_3$ (Rb: dark gray, Ca: gray and F: black). b) Brillouin zone of a simple cubic lattice

The full-potential linearized-augmented plane wave (FP-LAPW) method as implemented in the WIEN2k[12] code based on DFT[13] is used to describe the ground state. We have used three different approximations for the calculation of exchange-correlation energy functional, namely, the local density approximation (LDA)[14], the well- known generalized gradient approximation (GGA) of Perdew, Burke and Ernzerhof (PBE)[15] and the recently proposed GGA due to Wu and Cohen (WC)[16]. For calculating electronic and optical properties, only the WC scheme has been applied.

The lattice constants are calculated using Murnaghan's equation of state[17] while the bulk modulus (B_o) is calculated by fitting the pressure-volume data to a third-order Birch equation of state[18].

In order to achieve energy eigenvalues convergence, the wave functions in the interstitial region are expanded in plane-waves with a cut-off $K_{max} = 8/R_{MT}$, where R_{MT} is the smallest muffin-tin radius in the unit cell and K_{max} gives the magnitude of the largest K vector in the plane-wave expansion. The R_{MT} are taken to be 2.5, 1.9 and 2.0 (a.u.) for Rb, Ca and F, respectively. The valence wave functions inside muffin-tin spheres MT are expanded up to $l_{max} = 10$, while the charge density was Fourier expanded up to $G_{max} = 14$ (a.u.)$^{-1}$. The core energy cutoff is taken as −6.0 Ry. The calculations are performed with a (12×12×12) Monkhorst - Pack (MP) k-point mesh for the cubic structure corresponding to 56 k points in the (1/48) irreducible first Brillouin zone of the unit cell. The electronic structure calculations to obtain the partial densities of states (DOS) for all structures are performed using the tetrahedron method with Blöchl corrections[19]. The self-consistence calculations are considered to be converged only when the convergence tolerance of energy and charge are less than $0.1m$Ry and $0.1m$ electron charges, respectively.

In order to study the compound's optical properties, we must calculate the complex dielectric function $\varepsilon(\omega) = \varepsilon_1(\omega) + i\varepsilon_2(\omega)$, which describes the complete response of a material to the applied electromagnetic radiations field[20]. $\varepsilon_1(\omega)$ and $\varepsilon_2(\omega)$ are the real and imaginary parts of the dielectric function, respectively. The direct inter-band contributions to $\varepsilon_2(\omega)$ are calculated by considering all possible transitions from the occupied to the unoccupied states; taking the appropriate transition matrix element into account[21,22];

$$\varepsilon_2(\omega) = \left(\frac{\hbar^2 e^2}{\pi m^2 \omega^2}\right) \sum_{c,v} \int d^3k \ \langle c_k \mid p^{\alpha} \mid v_k \rangle \ \langle v_k \mid p^{\beta} \mid c_k \rangle \ \text{x} \ \delta(\varepsilon_{c_k} - \varepsilon_{v_k} - \omega) \quad (1)$$

Where p is the momentum matrix element between states of bands α and β with crystal momentum $\boldsymbol{k}$. c_k and v_k are the crystal wave functions corresponding to the conduction and the valance bands with crystal wave vector. Using the Kramers-Kroning relation[20], $\varepsilon_1(\omega)$ can be calculated from the imaginary part of dielectric function:

$$\varepsilon_1(\omega) = 1 + \frac{2}{\pi} P \int_0^{\infty} \frac{\omega' \varepsilon_2(\omega')}{(\omega')^2 - \omega^2} d\omega' \quad (2)$$

where P is the integral principle value.

The refractive index $n(\omega)$, the extinction coefficient $k(\omega)$, the absorption coefficient $I(\omega)$, and the reflectivity $R(\omega)$ in the crystal are given by[22-24]:

$$n(\omega) = \left[\frac{\sqrt{\varepsilon_1^2(\omega) + \varepsilon_2^2(\omega)} + \varepsilon_1(\omega)}{2}\right]^{1/2} \quad (3)$$

$$k(\omega) = \left[\frac{\sqrt{\varepsilon_1^2(\omega) + \varepsilon_2^2(\omega)} - \varepsilon_1(\omega)}{2}\right]^{1/2} \quad (4)$$

$$I(\omega) = \sqrt{2}\omega \left[\sqrt{\varepsilon_1^2(\omega) + \varepsilon_2^2(\omega)} - \varepsilon_1(\omega)\right]^{1/2} \quad (5)$$

$$R(\omega) = \frac{n + ik - 1}{n + ik + 1} \quad (6)$$

3. Results and Discussions

3.1. Structural Properties

In this subsection we aim to calculate the total energy as a function of unit-cell lattice parameter around the equilibrium cell lattice parameter a_0. In Figure 2, we presented the relation between the energy change and the lattice parameter a_0. The calculated total energies versus lattice parameter were fitted using Murnaghan's equation of state[17] to determine the other different important structural and ground state properties such as the bulk modulus B_0, the pressure derivative B'_o of the bulk modulus, and bond lengths. The calculated ground-state parameters (a_0, B_0, and B') for

crystalline $RbCaF_3$ are listed in Table 1 along with previous theoretical[25-27] and experimental values[28, 29].

Table 1. Lattice constant a(Å), bulk modulus B_o(GPa), bulk modulus derivative B', and bond lengths (Å)

	Calculated Current Investigation	Experimental	Theoretical
Lattice constant a(Å)	4.53[a], 4.45[b], 4.37[c]	4.455[d]	4.471[e], 4.483[f]
B_0(GPa)	46.6[a], 51.3[b], 59.3[c]	50.40[g]	47.275[f]
B_0'	5.1[a], 4.7[b], 0.3[c]		
Rb-F (Å)	3.200[a], 3.150[b], 3.089[c]		
Ca-F (Å)	2.263[a], 2.227[b], 2.185[c]	2.221[h]	

a) Present calculation GGA-WC.
b) Present calculation GGA-PBE.
c) Present calculation LDA.
d) Ref[25].
e) Ref[28].
f) Ref[29].
g) Ref[26].
h) Ref[27].

The computed lattice constant using (WC-GGA) is found slightly overestimated compared to the measured data. The lattice constant from our (WC -GGA) calculations is found 1.7% larger than the experimental values; on the other hand, when we used the (LDA) we found that the lattice constant is slightly underestimated compared with the experimentally measured data, while the LDA calculation is 1.9% smaller. In addition, we found that the (PBE-GGA) calculation agree well with the measured data, in fact its percentage difference compared with experimental value is about 0.1%. This is why we used the (PBE-GGA) method of exchange - correlation energy functional to calculate the electronic and optical properties of $RbCaF_3$ in the following subsections.

3.2. Electronic Properties

The band structure of the fluoroperovskite, $RbCaF_3$, is predicted along the high symmetry directions in the first Brillouin zone, as shown in Figure 1.b, where symmetry points are Γ (0, 0, 0), X (1, 0, 0), M (1, 1, 0) and R (1, 1, 1).

We calculated the band structure along these high symmetrical directions in the first Brillouin zone at the calculated equilibrium lattice parameter as shown in Figure 3. One can see that the valence band maximum lies at M symmetry point of the first Brillouin zone while the conduction band minimum lies at Γ symmetry point of first Brillouin zone, resulting in an indirect band gap (M- Γ).The calculated values of the band gap width (E_g) is 6.57 eV when using WC-GGA and LDA, but when using PBE-GGA the E_g is found = 6.38 eV. The previous experimental measurement for the E_g of $RbCaF_3$ was 10.9 eV[30]. A quick comparison between our calculated E_g value and the previously published one (10.9 eV) shows that the experimental value is 40% higher using PBE-GGA, WC-GGA and LDA approximations. This discrepancy can be related to insufficient accuracy in reproducing both exchange – correlation energy and its charge derivative. To the authors' best knowledge, the literature does not contain any theoretical results for E_g. Therefore, the calculated band gaps using PBE-GGA, WC-GGA and LDA are compared with the available experimental data and listed in Table 2.

Table 2. Calculated band gaps energy

	Calculated Current Investigation (eV)			Experimental data (eV)
	WC-GGA	PBE-GGA	LDA	
$E^{R-R}(eV)$	9.56	9.71	9.74	
$E^{\Gamma-\Gamma}(eV)$	6.53	6.69	6.66	
$E^{X-X}(eV)$	8.63	8.83	8.83	
$E^{M-M}(eV)$	9.23	9.47	9.61	
$E^{R-\Gamma}(eV)$	6.38	6.56	6.56	
$E^{X-\Gamma}(eV)$	6.63	6.79	6.76	
$E^{M-\Gamma}(eV)$	6.38	6.57	6.57	10.9[Ref[30]]

Total and partial density of states of the compounds is plotted in Figure 4. The large dispersion nature of the bands is very evident in the figure. The bands around (-23, -19.5, and -16.7) eV are occupied by Rb-4s, F-2s, and Ca-3p orbitals, respectively. The peak around -7.1 eV represents mainly the Rb-4p contribution. The top of valence band between the Fermi level (E_F) and -1.7 eV is primarily composed of the fluorine 2p. Finally, the conduction band which lies just above the Fermi level is partially occupied by the d states of both Ca and Rb.

3.3. Pressure Dependence of Band Gaps

In this subsection, we investigate the hydrostatic pressure effect on the energy gap and on the electronic properties of the semi-conductors. The pressure changes induced within the interatomic distances lead to changes in the covalent-bands charge-distributions and consequently affect all important parameters including the compounds' energy gaps.

The Murnaghan equation of state[17] was used to compress the unit cell. The variation of the lattice parameter with pressure is given by the equation:

$$p = \frac{B_0}{B_0'}\left[\left(\frac{V_0}{V}\right)^{B_0'} - 1\right]$$

Where B_0 is the bulk modulus, V_0 is the unit cell volume at ambient pressure, and B_0' represents the derivative of B_0 with respect to pressure.

Table 3. Calculated linear and quadratic pressure coefficient of high symmetry points band gap energy of $RbCaF_3$

	R-R	Γ-Γ	X-X	M-M
E(0)	9.53873	6.51507	8.61352	9.22196
a	0.07377	0.08511	0.09089	0.00995
b	-0.00125	-0.00107	-0.00155	0.00156

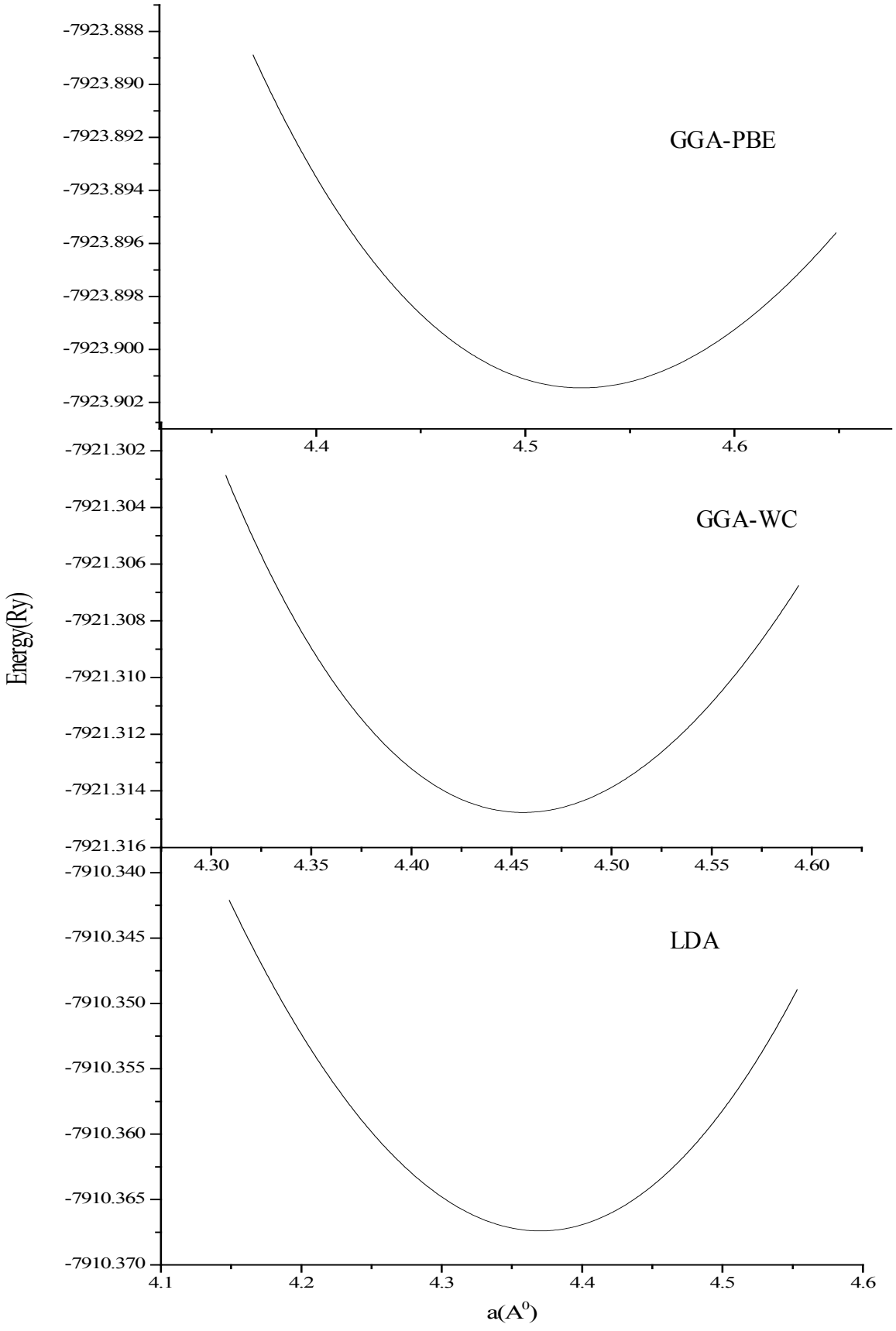

Figure 2. Total energy per atom as a function of lattice parameters (fluoroperovskite $RbCaF_3$ structure)

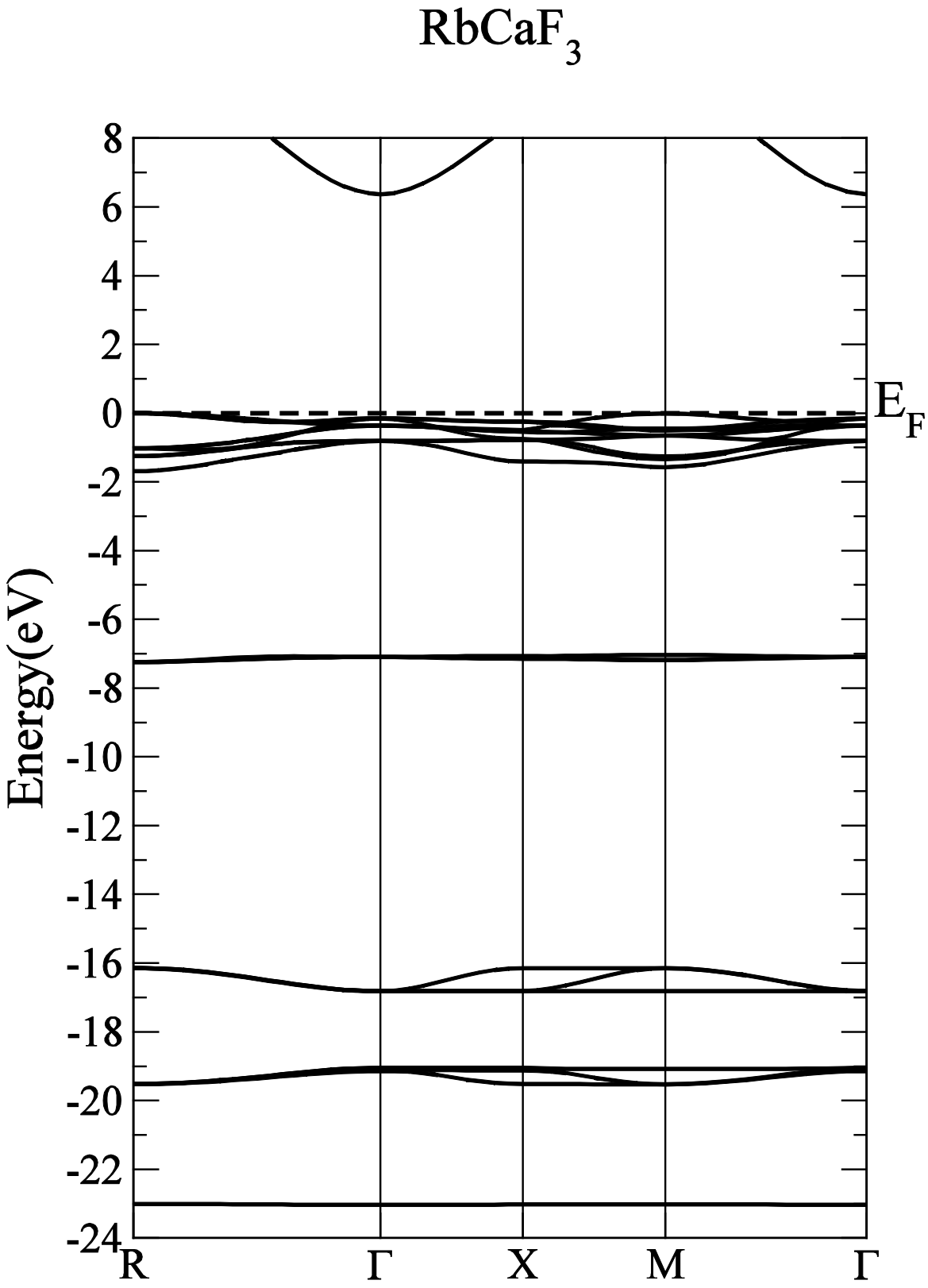

Figure 3. Energy band structure of $RbCaF_3$

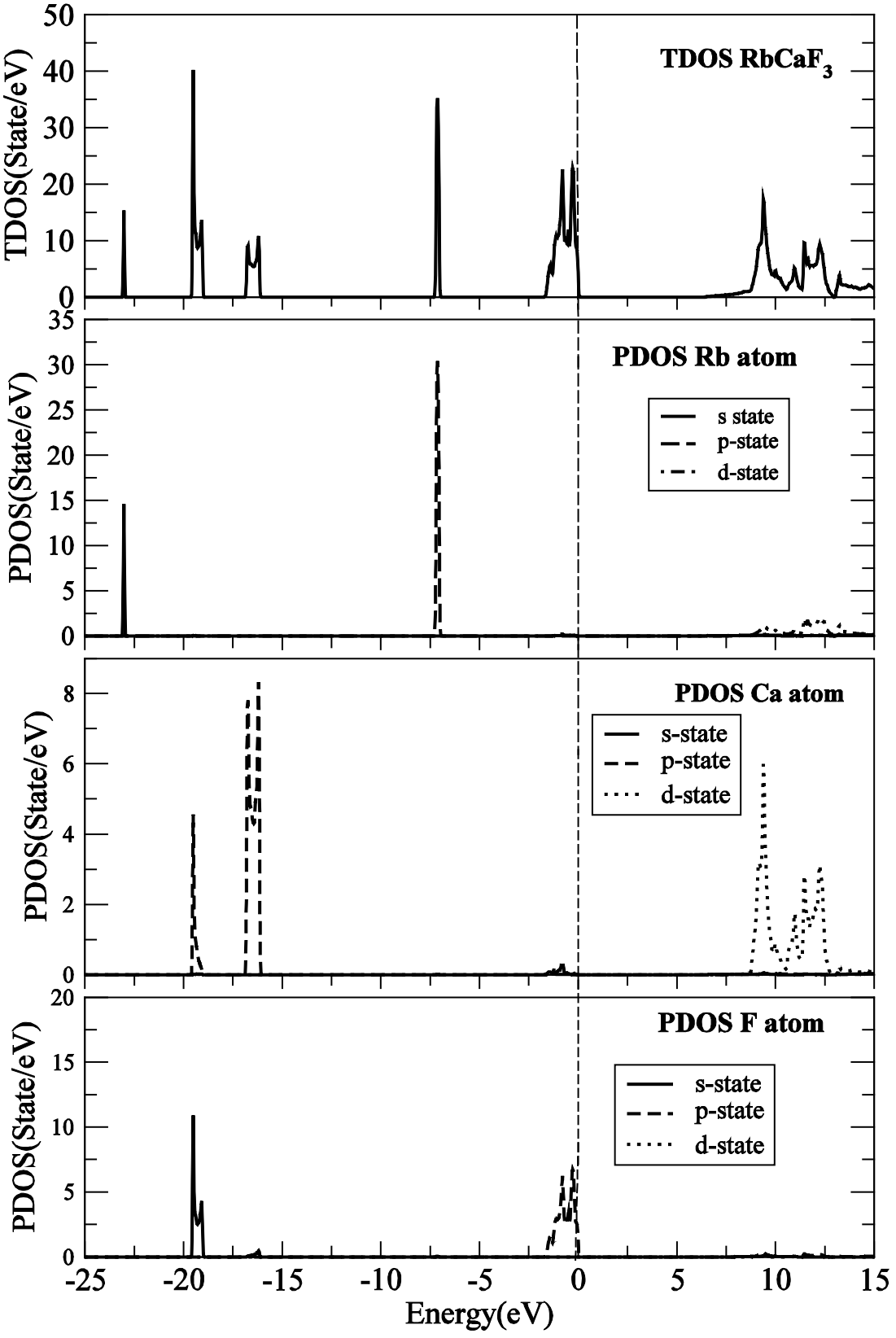

Figure 4. Total and partial DOS of $RbCaF_3$. The black, dashed and dotted lines refer to s-, p-, and d- states, respectively

The band energies at the symmetry points of $RbCaF_3$ were investigated as a function of hydrostatic pressure from 0 to 15GPa. $RbCaF_3$ band gap results based on the WC-GGA calculations versus pressure are shown in Figure 5. The data were fitted with the quadratic square fits to obtain the band gap pressure coefficients of the four main transitions. They are related by the expression:

$$E(p) = E(0) + ap + bp^2$$

The calculated values of the above equation are summarized in Table 3. Similar results can be observed from Figure 5 and Table 3 ($b \approx 0$) : the linear dependence can be seen in the four curves across the considered range of pressure.

Figure 6 displays the band gap energy variation of $RbCaF_3$ as a function of pressure. Note that, based on the PBE-GGA calculations, as the pressure increases from 0 to 15 GPa, the band gap energy increases monotonically from 6.38 to 7.76 eV.

Based on the relation:

$$E(p) = 6.358 + 0.0994p - 0.001p^2$$

The band gap changes from indirect to a direct one at 14 GPa, therefore, the band gap for $RbCaF_3$ becomes a direct at higher pressures (≥14GPa).

3.4. Optical Properties

In this subsection, the optical properties of $RbCaF_3$ are presented. The calculated real and imaginary parts of the dielectric function of $RbCaF_3$ at lattice constant equilibrium are shown in Figures 7 and 8.

As shown in Figure 7, the threshold energy of the dielectric function occurs at about 6.21eV. This threshold is due to the electronic transitions between the highest valance band F-2p and the lowest conduction band Ca-3d. Beyond threshold point, the curve increases sharply due to the abruptly increase in the number of points contributing toward $\varepsilon_2(\omega)$. The main peak in the spectrum is situated at 9.67eV. These peaks are dominated by transitions of electrons from the F-2p band and the small contribution of Ca-3p band just below Fermi energy to the unoccupied state of conduction band.

Pursuant to the Kramers-Kronig dispersion relation, the real part $\varepsilon_1(\omega)$ of dielectric function is displayed in Figure 8. The calculated static dielectric constant $\varepsilon_1(0)$ is at about 2.12, our calculated $\varepsilon_1(0)$ is more than the previous experimental measurement (1.90)[31] by 10%. The deviation of the calculated values from the experimental ones could be explained based on the temperature difference knowing that all theoretical calculations are done at 0K. The main peak is located at about 9.27 eV.

The curve reflects an increase, then decrease, followed by an increase in $\varepsilon_1(\omega)$ within the negative values; followed by a slow increase toward zero at high energy. The $\varepsilon_1(\omega)$ have a minimum value around 26.33eV.

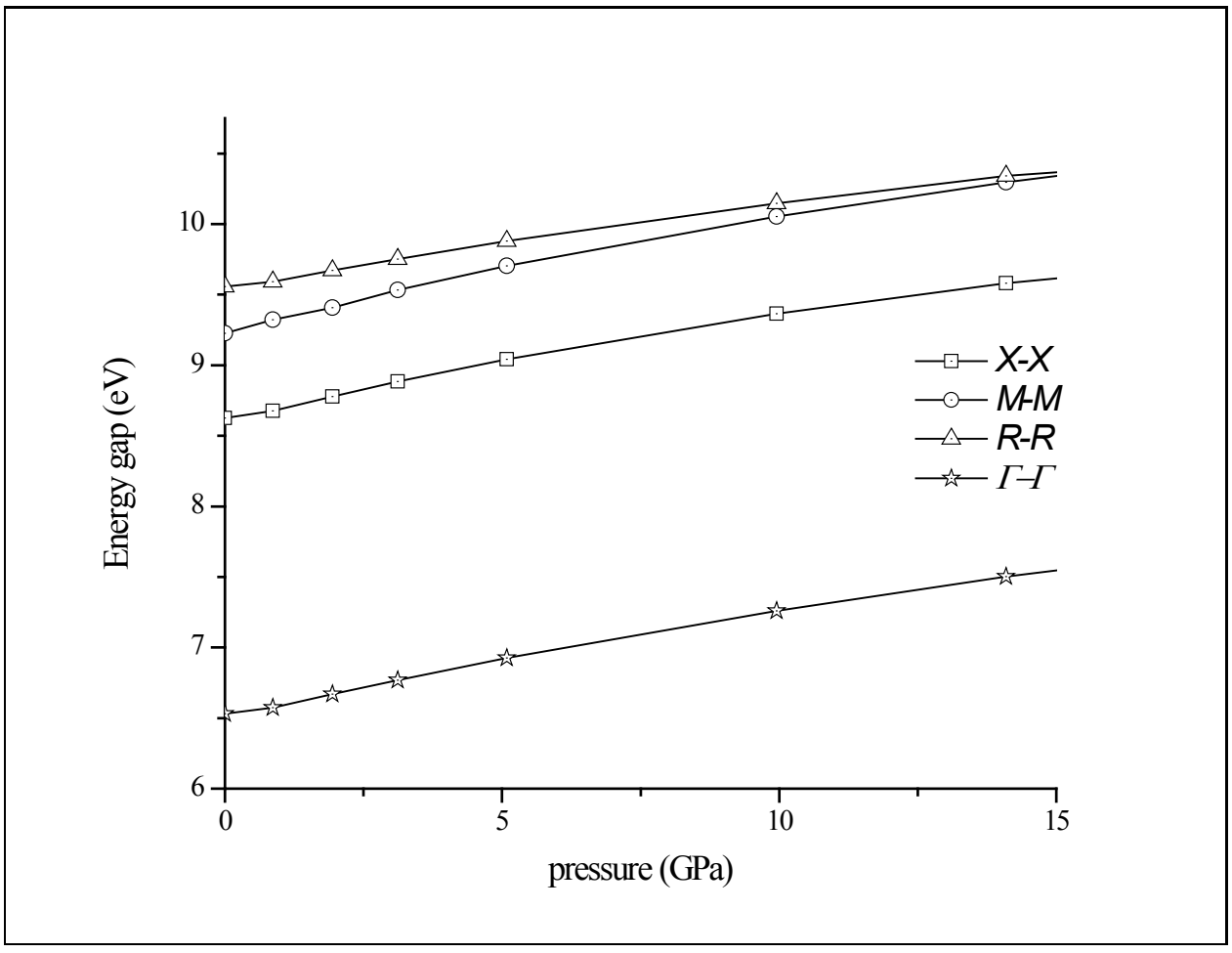

Figure 5. Calculated band gaps energy of $RbCaF_3$ at high symmetry points under varying hydrostatic pressure

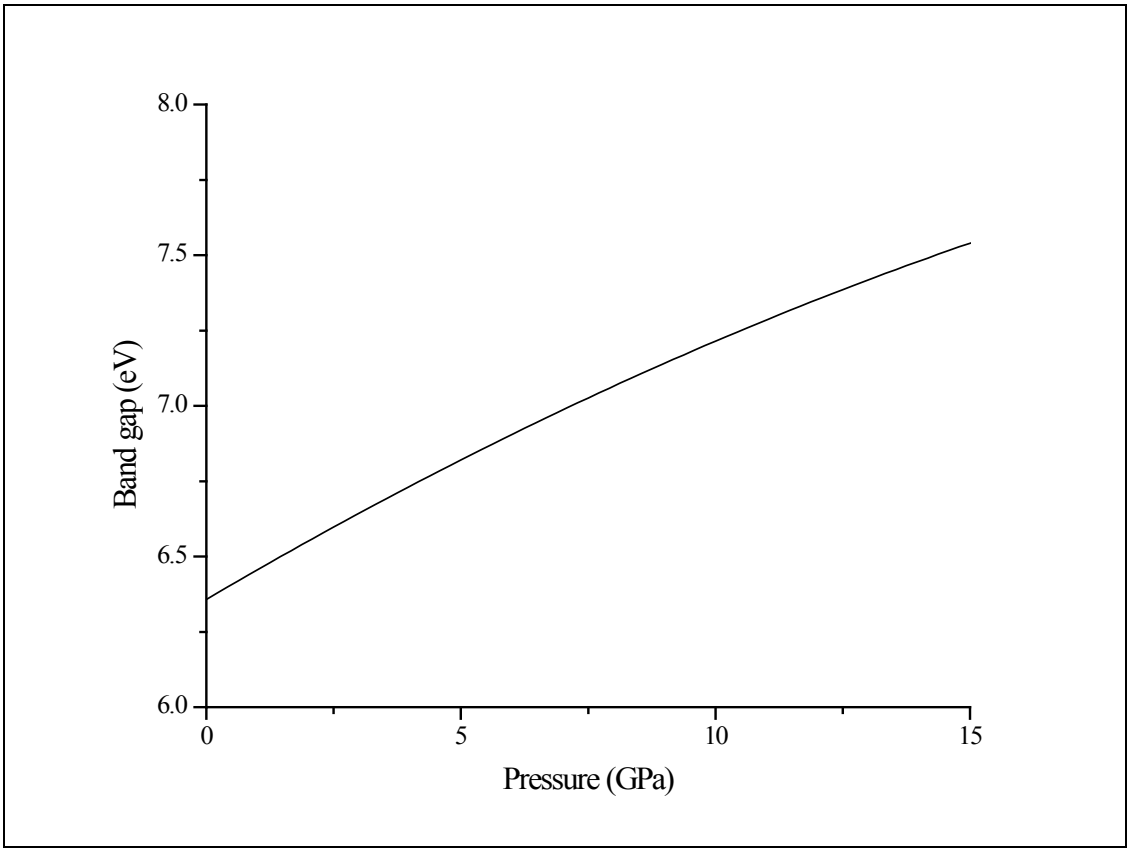

Figure 6. Calculated indirect band gaps energy of $RbCaF_3$ under varying hydrostatic pressure

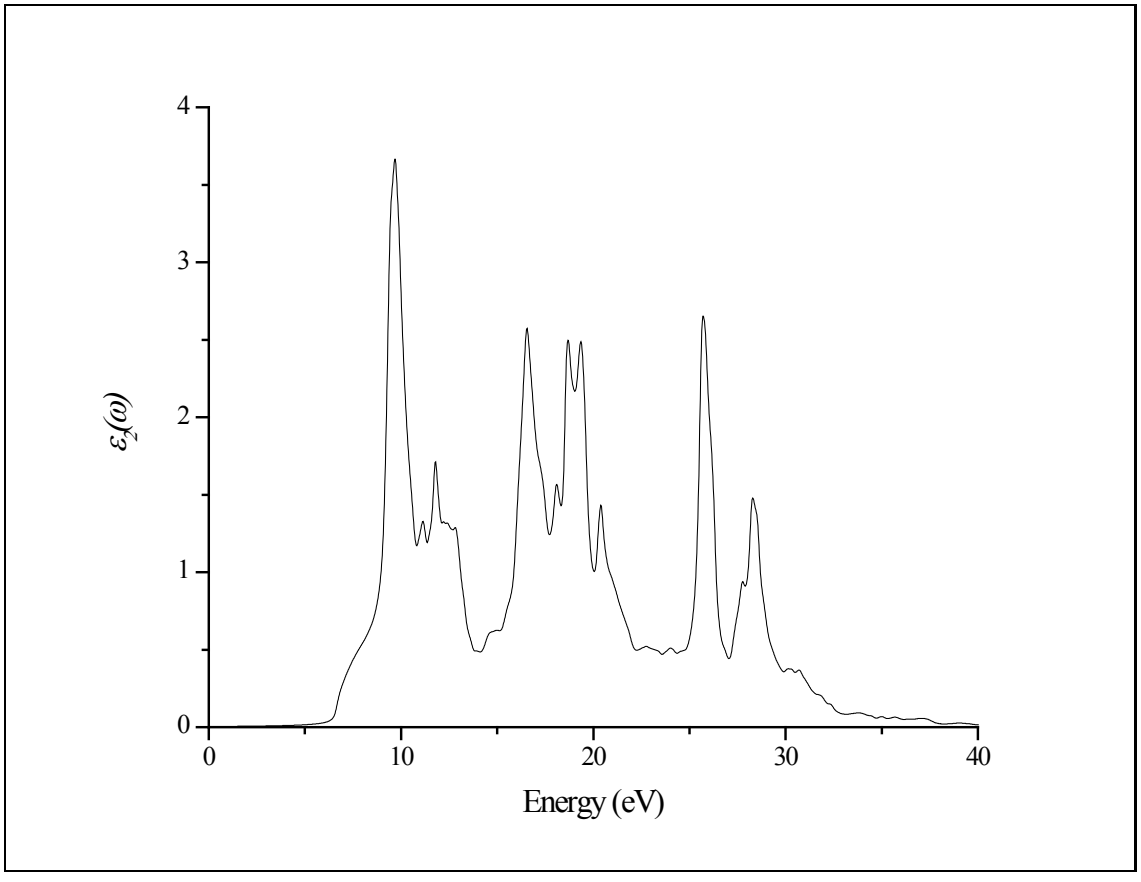

Figure 7. Calculated imaginary part $\varepsilon_2(\omega)$ of the dielectric function $\varepsilon(\omega)$

The other optical properties including the refractive indices $n(\omega)$, the extinction coefficient $k(\omega)$, the absorption coefficient $I(\omega)$, and the reflectivity $R(\omega)$ are calculated using $\varepsilon_1(\omega)$ and $\varepsilon_2(\omega)$ from equations[4-7].

The refractive index $n(\omega)$ is displayed in Figure 9 along xx-direction. The refractive index at zero energy is called the static refractive index and noted by $n(0)$. The calculated $n(0)$ is found to be 1.46. The refractive index reaches a maximum value of about 2.16 at 9.32 eV.

The extinction coefficient $k(\omega)$ have been calculated as shown in Figure 10 along xx-direction. The local maxima of the $k(\omega)$ correspond to the zero of $\varepsilon_1(\omega)$ equals 1.09 at 19.52eV.

In Figure 11, we considered the reflectivity spectrum *R(ω)* along xx-direction. The zero frequency limits of the spectra *R(0)* is 3.05%. It stays below 10% up to 15 eV. However, at 9.7eV, the reflectivity spectrum has a local maximum of about 18%. It is created from the transition of the F-2p states of the valance band to the Ca-3d states of conduction band. This could be an indicative that the materials are highly transparent in the infrared, visible, and low frequency ultraviolet region of the energy spectrum. This is indicative that these materials could be of great interest as transparent coatings for efficient lenses. Beyond 15 eV, reflectivity increases with noticeable variations as it reaches a maximum value of 30.4% at 26.38 eV.

The absorption coefficient *I(ω)* is investigated and presented in Figure 12. The maximum absorption coefficient is found close to 2.73% at 25.92eV. The studied materials show weak absorption. The calculated absorption and reflectivity coefficients in this investigation show an appreciable amount of isotropy at low and high energies.

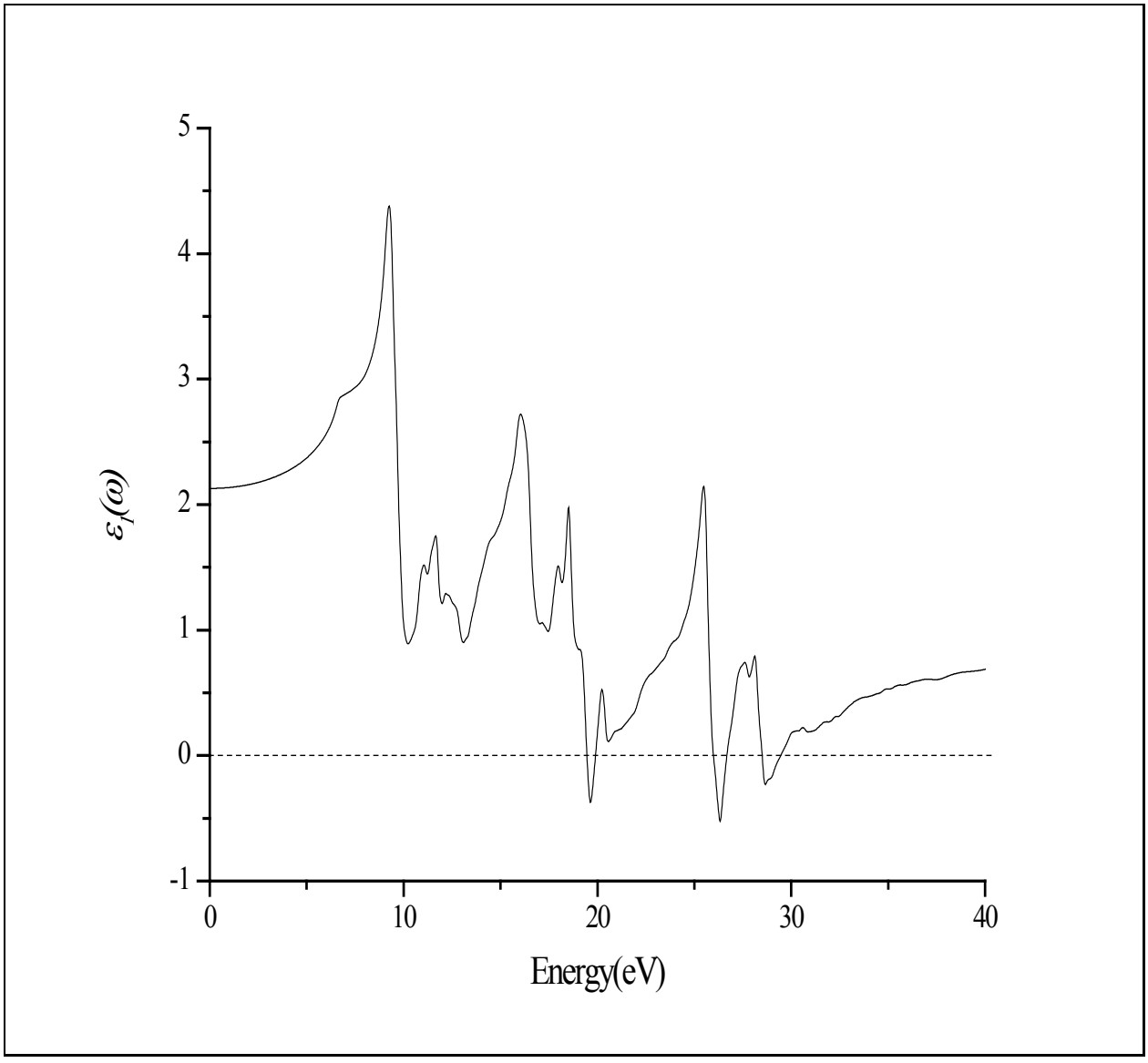

Figure 8. Calculated real part $\varepsilon_1(\omega)$ of the dielectric function $\varepsilon(\omega)$

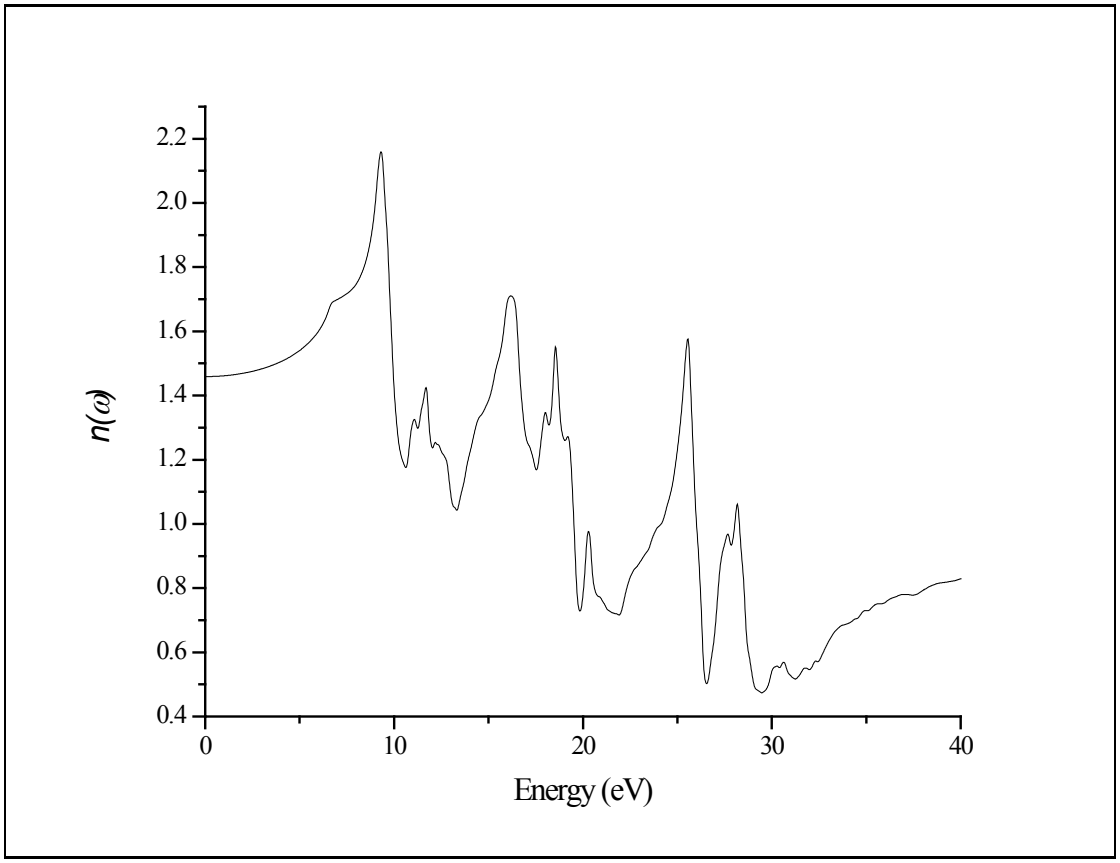

Figure 9. Calculated refractive index $n(\omega)$ of the dielectric function $\varepsilon(\omega)$

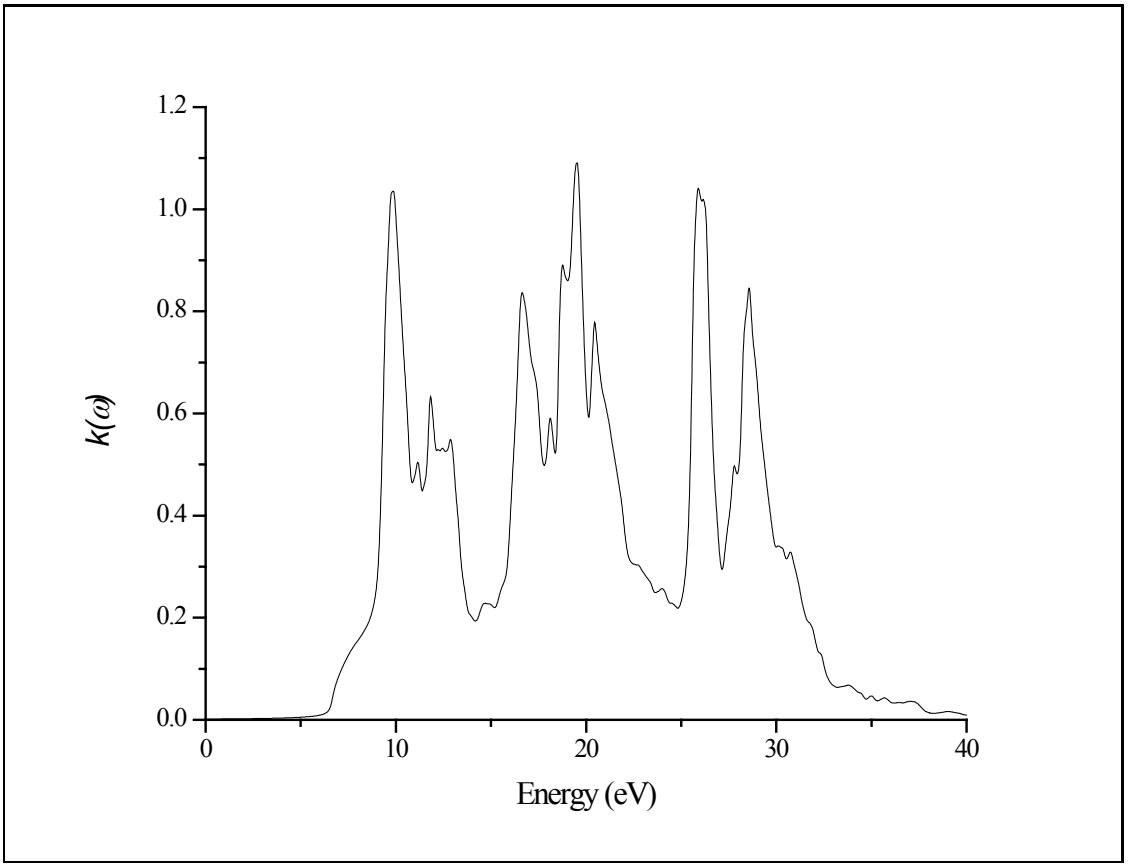

Figure 10. Calculated extinction coefficient $k(\omega)$ of the dielectric function $\varepsilon(\omega)$

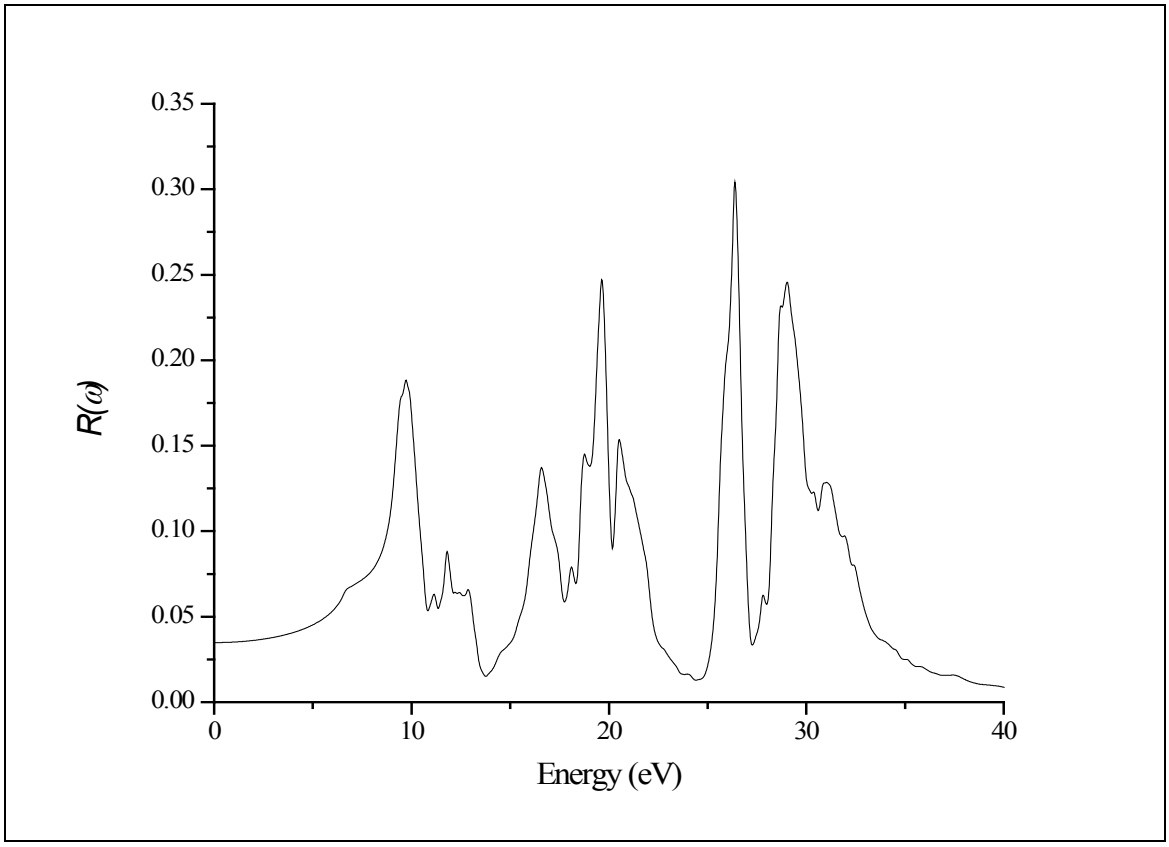

Figure 11. Calculated absorption coefficient $I(\omega)$ of the dielectric function $\varepsilon(\omega)$

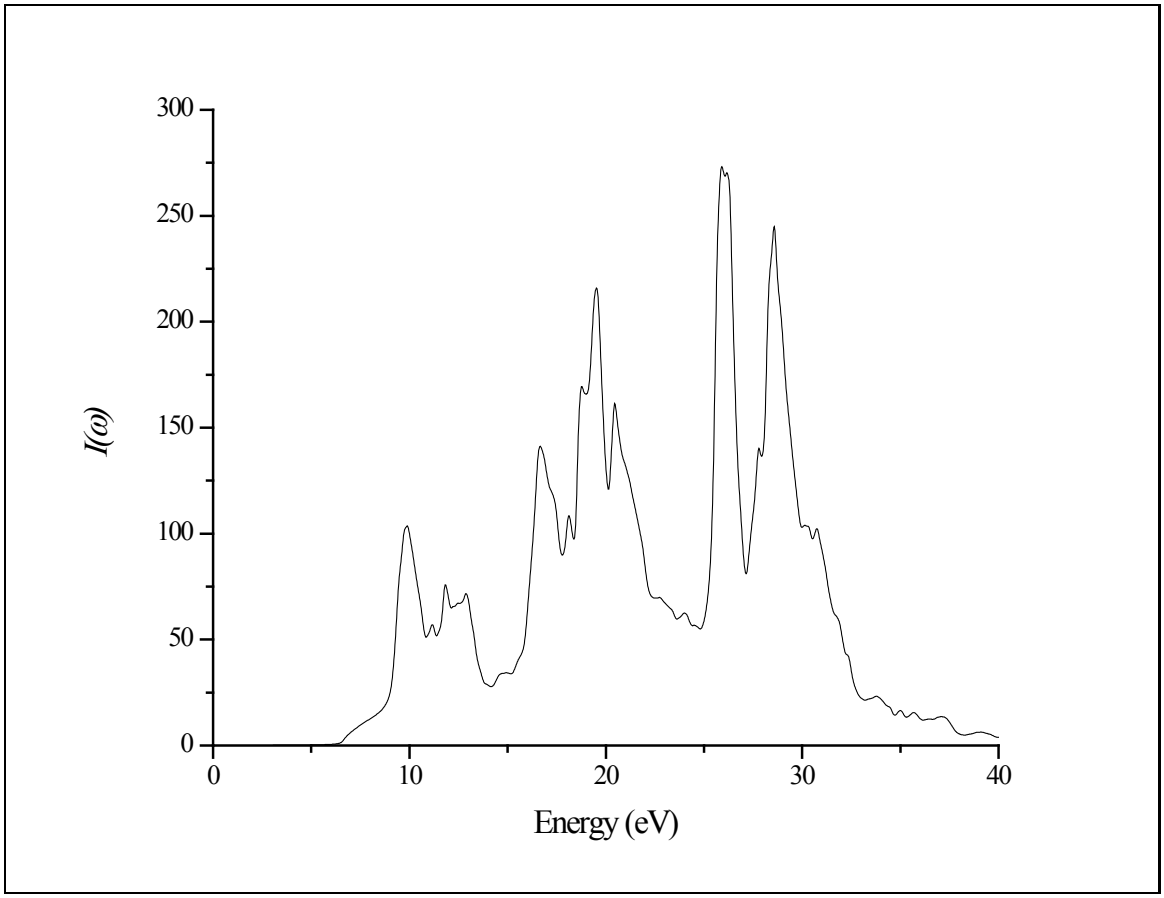

Figure 12. Calculated reflectivity coefficient $R(\omega)$ of the dielectric function $\varepsilon(\omega)$

4. Conclusions

The structural, electronic and optical properties of the $RbCaF_3$ are studied using the FP-LAPW method based on the density functional theory with three different approximations for the calculation of exchange-correlation energy functional; WC-GGA, PBE-GGA and LDA. The lattice constants and the bulk modulus are found to compare well with the available previous study. Our calculations show that the $RbCaF_3$ structure has an indirect energy band-gap at the Γ-M points in the Brillouin zoon. The relation between the energy gap and pressure based on this study is found linear, especially in the range 0-15GPa. The calculations conducted in this study revealed that the indirect gap of the $RbCaF_3$ structure transforms to a direct gap at 14 GPa. The real $\varepsilon_1(\omega)$ and the imaginary $\varepsilon_2(\omega)$ parts of the dielectric function is calculated. The calculated projected DOS and band structure were used to analyze the optical transitions. Finally, the refractive index $n(\omega)$, the extinction coefficient $k(\omega)$, the absorption coefficient $I(\omega)$, and the reflectivity $R(\omega)$ have also been calculated and presented.

REFERENCES

[1] H.K. Juwhari, M.H. Kilani, B.I. Lahlouh, S.A. Abedrabbo, K.A. Saleh, W.B. White, Mater Lett. 87, 80-83 (2012).

[2] H.K. Juwhari, W.B. White, Mater Lett. 64, (15) 1751-1755 (2010).

[3] T. Nishimatsu, N. Terakubo, H. Mizuseki, Y. Kawazoe, D.A. Pawlak, K. Shimamura, T. Fukuda, Jpn. J. Appl. Phys. 41 (2002) L365.

[4] C. Dotzler, G.V.M. Williams, A. Edgar, Curr. Appl. Phys. 8 (2008) 447.

[5] A. Kulkarni, F.T. Ciacchi, S. Giddey, C. Munnings, S.P.S. Badwal, J.A. Kimpton, D. Fini. International Journal of Hydrogen Energy 37 (24): (2012).

[6] J. M. D. Coey, M. Viret, S. von Molnar. Advances in Physics 48 (2), 167-293(1999).

[7] A. Bouamrane, J. P. Bastide, y L. Belkbir. C. R. Acad. Sci. Paris, t312:1287-1291, (1991).

[8] W. L. W. Ludekens y A. J. E. Welch. Acta Cryst., 5:841, (1952).

[9] K. Shimamura, N. Mujilatu, K. Nakano, S.L. Baldochi, Z. Liu, H. Ohtake, N. Sarukura, T. Fukuda, J. Cryst. Growth 197 (1999) 896.

[10] K. Shimamura, T. Fujita, H. Sato, A. Bensalah, N. Sarukura, T. Fukuda, Jpn. J. Appl. Phys. 39 (2000) 6807.

[11] A. Bensalah, K. Shimamura, T. Fujita, H. Sato, M. Nikl, T. Fukuda, J. Alloys Compd. 348 (2003) 258.

[12] P. Blaha, K. Schwarz, G.K.H. Madsen, D. Kvasnika and J. Luitz, WIEN2k, Technical Universität Wien: Austria, (2001); ISBN 3-9501031-1-2.

[13] P. Hohenberg, and W. Kohn, Phys. Rev. B 136, 864 (1964).

[14] J. P. Perdew and A. Zunger, Phys. Rev. B., 1981, 23, 5048.

[15] J.P. Perdew, K. Burke, and M. Ernzerhof, Phys. Rev. Lett. 77, 3865 (1996).

[16] Z. Wu, R.E. Cohen, Phys. Rev. B 73 (2006) 235116.

[17] F.D. Murnaghan, Proc. Nat. Acad. Sci. USA. 30, 244 (1944).

[18] F. Birch, J. Geophys. Res. 83, 1257 (1987).

[19] P. Blochl, O. Jepsen, O.K. Andersen, Phys. Rev. B 49, 16223 (1994).

[20] F.Wooten, Optical Properties of Solids, Academic Press, New York, (1972).

[21] S. Kumar, T.K. Maury, S. Auluck, J. Phys. Condens. Matter, 20, 075205.

[22] M. Fox, Optical Properties of Solids, Oxford University Press, New York,(2001).

[23] M. Dreesel, G.Gruner, Electrodynamics of solid: Optical Properties of Electrons in Matter, Cambridge University Press, UK, (2002).

[24] Ahmad A. Mousa, Nada T. Mahmoud, Jamil M. Khalifeh, Comput. Mater. Sci, 79, 201-205, (2013).

[25] A. Bulou, C. Ridou, M. Rousseau, J. Nouet, A. Hewat, J. Phys. 41 (1980) 87.

[26] F. Wooten, Optical Properties of Solids, Academic Press, New York, 1972.

[27] G. Murtaza, I. Ahmad, B. Amin, A. Afaq, M. Maqbool, J. Maqssod, I. Khan, M. Zahid, Opt. Mater. 33 (2011) 553.

[28] L.Q. Jiang, J.K. Guo, H.B. Liu, M. Zhu, X. Zhou, P. Wu, C.H. Li, J. Phys. Chem. Solids 67 (2006) 1531.

[29] V. Luafza, A. Costales, A.M. Pendbs, M. Florez, V.M.G. Fembndez, Solid State Commun. 104 (1997) 47.

[30] A.N. Belsky, P. Chevallier, E.N. Melchakov, C. Pedrini, P.A. Rodnyi, A.N. Vasilev, Chem. Phys. Lett. 278 (1997) 369.

[31] C. Ridou, M. Rousseaut, F. Gervais, J. Phys. C Solid State Phys. 19 (1986) 5757.